

General Control for Boost PFC Converter from a Sliding Mode Viewpoint

Grace Chu, Siew-Chong Tan, Chi K. Tse and Siu Chung Wong

Department of Electronic and Information Engineering, Hong Kong Polytechnic University, Hong Kong

email: grace@eie.polyu.edu.hk

Abstract—In this paper, we propose a current control methodology for the boost PFC converter based on sliding mode control theory. The resulting control is very general in the sense that it provides input current tracking under all practical conditions by systematically including all necessary control functions that compensate for the possible nonlinearity such as the zero-crossing distortion in high line frequency condition. By choosing suitable state control variables and a proper sliding surface, the derivation arrives at a feedforward control which is similar to a previously proposed method. The implementation takes the form of a typical pulse-width modulation (PWM) control. It can be designed either as an individual current controller or as feedforward control applied to a standard PFC controller.

I. INTRODUCTION

In this paper, a general current control rule is derived for the boost PFC converter. The aim is to provide input current tracking under all practical conditions. Specifically, the proposed general control systematically and automatically includes the necessary compensation functions to eliminate the phenomena due to the inherent nonlinearity, which may manifest as zero-crossing distortion under certain line frequency condition [1]. The derivation is based on general sliding mode (SM) control theory. A fixed-frequency version of sliding mode control [2] is employed and the resulting control takes the form of a typical PWM control, which can be readily implemented with analog circuits. Interestingly, this SM-based derivation is simpler and more straight forward than the conventional large signal approach, as complicated current loop modeling is not required. The resulting general control scheme turns out to be consistent with some voltage feedforward schemes proposed previously, with all the required feedforward signal paths included systematically [4], [5]. SM operation is ensured by the existence condition and stability of the current loop can be assessed by frequency response analysis. Experimental measurements are presented to verify the analytical results.

II. THEORETICAL DERIVATION

In this section, a general current loop control rule for the boost PFC converter is derived. Conventional linear control is adopted for the outer voltage loop to regulate the output voltage and to generate the half-sinusoidal reference current. Continuous conduction mode (CCM) is considered here as it is commonly used in medium to high power applications. A simplified schematic is shown in Fig. 1

A. Deciding the Control State Variables

The proposed current controller employs the current error, x_1 , the integral of the current error, x_2 , and the double

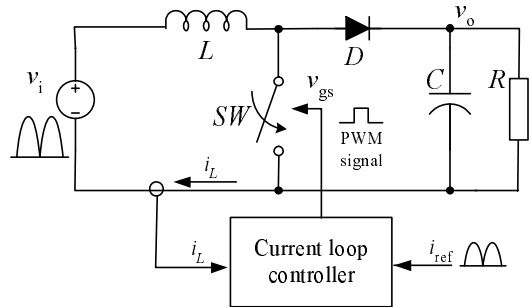


Fig. 1. A boost PFC converter with a general current controller for the inner current loop.

integral of the current error, x_3 , as the controlled state variables. The double-integral term is included to further alleviate the steady-state error caused by the finite switching frequency [3]. The state variables are described as

$$x_1 = i_{\text{ref}} - i_L; \quad x_2 = \int x_1 dt; \quad x_3 = \int \int x_1 dt dt, \quad (1)$$

where i_L denotes the instantaneous inductor current and i_{ref} represent the reference input current, as shown in Fig. 1.

The switching function is defined as:

$$u = \frac{1}{2}(1 + \text{sign}(S)) \quad (2)$$

where u represents the logic state of the power switch.

B. Deciding the Sliding Surface

The state variables trajectory is defined as a linear combination of the state variables, i.e.,

$$S = \alpha_1 x_1 + \alpha_2 x_2 + \alpha_3 x_3 \quad (3)$$

where α_1 , α_2 and α_3 represent the sliding mode coefficients. The sliding surface is defined by setting $S = 0$, i.e.,

$$\alpha_1 x_1 + \alpha_2 x_2 + \alpha_3 x_3 = 0. \quad (4)$$

Considering that the boost converter is operating in CCM, the time differentiation of (1) gives the dynamic model of the proposed system as

$$\dot{x}_1 = \frac{d}{dt} i_{\text{ref}} - \frac{1}{L}(v_i - \bar{u}v_o); \quad \dot{x}_2 = x_1; \quad \dot{x}_3 = x_2, \quad (5)$$

where $\bar{u} = 1 - u$ represents the inverse logic of u , and v_i denotes the rectified input voltage. Under the invariance of SM control, $S = 0$ and $\dot{S} = 0$. Thus,

$$\dot{S} = \alpha_1 \dot{x}_1 + \alpha_2 \dot{x}_2 + \alpha_3 \dot{x}_3 = 0. \quad (6)$$

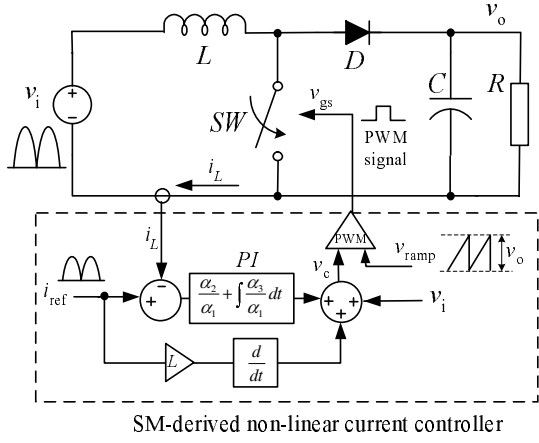


Fig. 2. A boost PFC converter with the current loop employing the proposed general control rule.

C. Synthesizing the Control Signal by Equivalent Control

Under the equivalent control, the logic signal \bar{u} is substituted by the continuous signal \bar{u}_{eq} , such that

$$0 < \bar{u}_{eq} < 1. \quad (7)$$

Substituting (5) and (6) into (7) gives

$$\alpha_1 \frac{di_{ref}}{dt} - \frac{\alpha_1}{L}(v_i - \bar{u}_{eq}v_o) + \alpha_2(i_{ref} - i_L) + \alpha_3 \int (i_{ref} - i_L)dt = 0. \quad (8)$$

Solving (8) for \bar{u}_{eq} gives

$$\bar{u}_{eq} = \frac{1}{v_o} \left[-\frac{Ldi_{ref}}{dt} + v_i - LK_1x_1 - LK_2x_2 \right] \quad (9)$$

where

$$K_1 = \frac{\alpha_2}{\alpha_1}; K_2 = \frac{\alpha_3}{\alpha_1}.$$

Equation (9) is a general control rule for the boost PFC converter and is illustrated in Fig. 2.

III. EXISTENCE CONDITION

For sliding mode operation to occur, the existence condition has to be satisfied, i.e., $\lim_{S \rightarrow 0} S \cdot \dot{S} < 0$.

For $S > 0$, i.e., $u = 1$, $\bar{u} = 0$ and $\dot{S} < 0$, we have

$$\alpha_1 \frac{di_{ref}}{dt} - \frac{\alpha_1}{L}v_i + \alpha_2x_1 + \alpha_3x_2 < 0. \quad (10)$$

For $S < 0$, i.e., $u = 0$, $\bar{u} = 1$ and $\dot{S} > 0$, we have

$$\alpha_1 \frac{di_{ref}}{dt} - \frac{\alpha_1}{L}(v_i - v_o) + \alpha_2x_1 + \alpha_3x_2 > 0. \quad (11)$$

The derivative of the reference current can be obtained as

$$\frac{di_{ref}}{dt} = \frac{2V_{ref}^2}{RV_i} \frac{d \sin(\omega t)}{dt} = \frac{2V_{ref}^2}{RV_i} \omega \cos(\omega t), \quad (12)$$

where ω is the line frequency in rads^{-1} . Here we assume $v_o = V_{ref}$ and the converter has a very high efficiency η with $\eta \approx 1$.

Substituting (12) into (10) and (11), and re-arranging, the existence condition becomes

$$K_1x_1 + K_2x_2 < -\frac{2V_{ref}^2}{RV_i} \omega \cos(\omega t) + \frac{V_i}{L} \sin(\omega t) \\ K_1x_1 + K_2x_2 > -\frac{2V_{ref}^2}{RV_i} \omega \cos(\omega t) + \frac{V_i}{L} \sin(\omega t) - \frac{V_{ref}}{L}. \quad (13)$$

In the right hand side of (13), x_1 is the current error which is basically the inverted function of the inductor current ripple and x_2 is the integral of the current error. The right hand sides of (13) define the upper and lower boundaries for the amplified current error and its integral. Thus, satisfaction of the existence condition can be verified numerically by plotting the existence condition boundaries along with the current error and its integral for a rectified line cycle.

IV. FREQUENCY RESPONSE ANALYSIS

Under the assumption of ideal sliding mode operation, the current loop behavior is confined to the sliding surface $S = 0$ defined in (4) and the dynamics of the system can be described by $\dot{S} = 0$ in (6). Re-arranging (6) gives

$$\frac{di_L}{dt} = \frac{di_{ref}}{dt} + K_1(i_{ref} - i_L) - K_2 \int (i_{ref} - i_L)dt. \quad (14)$$

Due to the linear nature, (14) can be readily expressed in s -domain as

$$si_L = si_{ref} + (i_{ref} - i_L) \left(K_1 + K_2 \frac{1}{s} \right). \quad (15)$$

The block diagram of (15) is depicted in Fig. 3 (a), which can be manipulated into a general form as shown in Fig. 3 (b). Upon inspection of Fig. 3 (b), the round-trip (open-loop) loop gain is obtained as

$$G(s) = \frac{1}{s} \left(K_1 + K_2 \frac{1}{s} \right) = \frac{K_2 \left(1 + \frac{K_1}{K_2} s \right)}{s^2}, \quad (16)$$

which is a second-order system with dc gain of K_2 and a zero at $\frac{K_2}{K_1} \text{ rads}^{-1}$. In practice, the round-trip loop gain is

$$G'(s) = G(s) \cdot H(s), \quad (17)$$

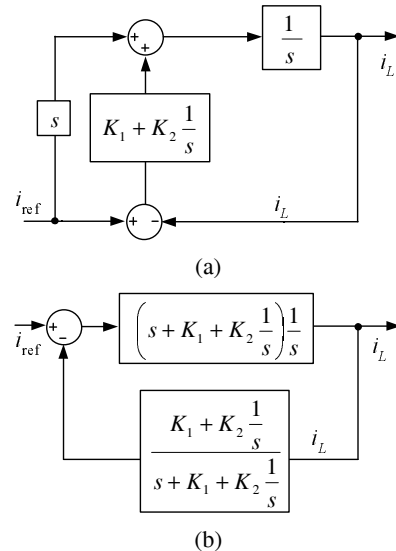


Fig. 3. (a) Block diagram of the current loop under the general control rule; (b) current loop block diagram in general form.

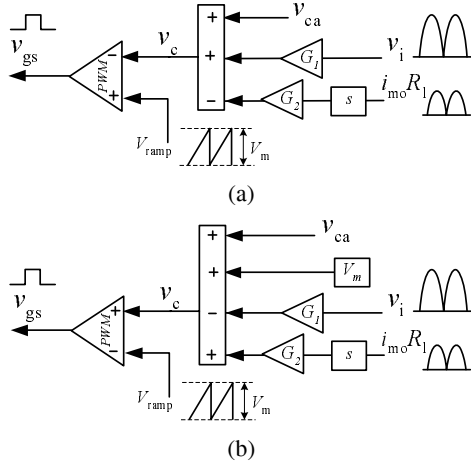


Fig. 4. Implementation of feedforward control for (a) a LEM controller; (b) a TEM controller.

where $H(s)$ accounts for the non-ideal properties of the power converter and the practical op-amps, such as the non-ideal integral and the limited dc gain, which will be discussed in detail in the following section.

V. IMPLEMENTATION

The resulting general control rule is readily implemented by discrete components as an individual current controller. Alternatively, it can be incorporated in standard PFC controllers, such as UC3854 and UCC3817, as an extra feedforward control. To formulate the feedforward control, the current variables $i_L - i_{ref}$ in (9) is replaced by the equivalent voltages across the sensing resistance $R_s i_L - R_l i_{mo}$, where i_{mo} is the current generated by the practical multiplier. The instantaneous output voltage v_o is approximated by the constant reference voltage V_{ref} .

In doing so, all the integrators in (16) are non-ideal and thus the first two poles are non-zero. Here we denote the frequencies of the first two poles by f_{p1} and f_{p2} . Besides, the dc gain is limited by the open-loop gain A_o of practical op-amps. For feasible implementation, a low-pass filter with pole frequency f_{p3} is inserted for filtering noise of frequency higher than half the converter switching frequency. Therefore, the practical loop gain transfer function becomes

$$G'(s) = \frac{A_o \left(1 + \frac{K_1}{K_2} s\right)}{\left(1 + \frac{s}{2\pi f_{p1}}\right) \left(1 + \frac{s}{2\pi f_{p2}}\right) \left(1 + \frac{s}{2\pi f_{p3}}\right)}, \quad (18)$$

where f_{p1} and A_o can be obtained analytically based on the op-amp's open-loop characteristics provided in the datasheet; f_{p2} is approximately calculated by $\frac{r_l + R_s}{L}$ rads^{-1} ; and r_l and R_s are the damping resistance and current sensing resistance of L respectively. Experimental frequency responses measured from our circuit (Figs. 5, 6 and Table I) give $f_{p1} \approx 10$ Hz, $f_{p2} \approx 59$ Hz, $f_{p3} \approx 64$ kHz and $A_o \approx 90$ dB. Based on (18), Bode plots can be obtained by drawing asymptotes manually or using softwares such as Matlab. Therefore, the SM coefficients can be selected by the desired crossover frequency and phase margin, as in the conventional Bode plots design approach used in linear controllers [6].

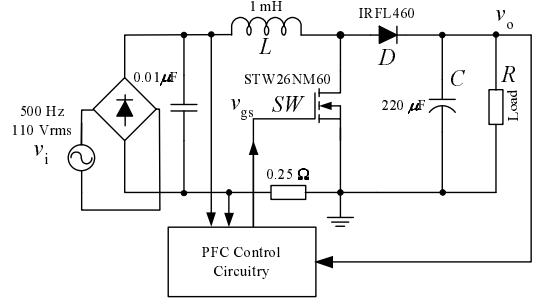


Fig. 6. Schematic of the boost PFC converter.

The equivalent control signal for leading edge modulation (LEM) is denoted by \bar{u}'_{eq} and is given by

$$\bar{u}'_{eq} = \frac{1}{V_{ref} R_s} \left[-\frac{L R_l di_{mo}}{dt} + R_s v_i - L K_1 (R_l i_{mo} - R_s i_L) - L K_2 \int (R_l i_{mo} - R_s i_L) dt \right]. \quad (19)$$

The control voltage v_c is obtained by multiplying (19) with the amplitude of the ramp function V_m , giving

$$v_c = \frac{V_m}{V_{ref}} v_i - \frac{V_m L R_l}{V_{ref} R_s} \frac{di_{mo}}{dt} - L K_1 \frac{V_m}{V_{ref} R_s} (R_l i_{mo} - R_s i_L) - L K_2 \frac{V_m}{V_{ref} R_s} \int (R_l i_{mo} - R_s i_L) dt. \quad (20)$$

On the other hand, the current amplifier output of a LEM controller, e.g. UCC3817, can be expressed as

$$v_{ca} = (R_s i_L - R_l i_{mo}) H_{ca}, \quad (21)$$

where H_{ca} is the transfer function of a type 2 amplifier, which can be expressed in the s -domain as

$$H_{ca} = \frac{R_f}{R_l} + \frac{1}{R_l C_z s}, \quad (22)$$

where R_f , R_l and C_z are the component values shown in Fig. 5. Here the high-frequency pole for noise filtering is ignored. If we design the component values such that

$$\frac{R_f}{R_l} = \frac{V_m L}{R_s V_{ref}} K_1; \quad \frac{1}{R_l C_z} = \frac{V_m L}{R_s V_{ref}} K_2, \quad (23)$$

the general control rule can be implemented as a kind of feedforward control scheme for a LEM controller. Simplifying (20) with consideration of (21)–(23) gives

$$v_c = G_1 v_i - s G_2 R_l i_{mo} + v_{ca}, \quad (24)$$

where $G_1 = \frac{V_m}{V_{ref}}$ and $G_2 = \frac{V_m L}{V_{ref} R_s}$. The resulting feedforward control is illustrated in Fig. 4(a) and it is consistent with that proposed in [5].

Alternatively, the general control rule is readily applied to a trailing edge modulation (TEM) controller. The current amplifier output of a TEM controller can be represented by

$$v_{ca} = (R_l i_{mo} - R_s i_L)(1 + H_{ca}) \approx (R_l i_{mo} - R_s i_L) H_{ca}. \quad (25)$$

Following a similar procedure as that for LEM, the feedforward control scheme for a TEM controller can be obtained as

$$v_c = V_m - G_1 v_i + s G_2 R_l i_{mo} + v_{ca}, \quad (26)$$

which is illustrated in Fig. 4 (b).

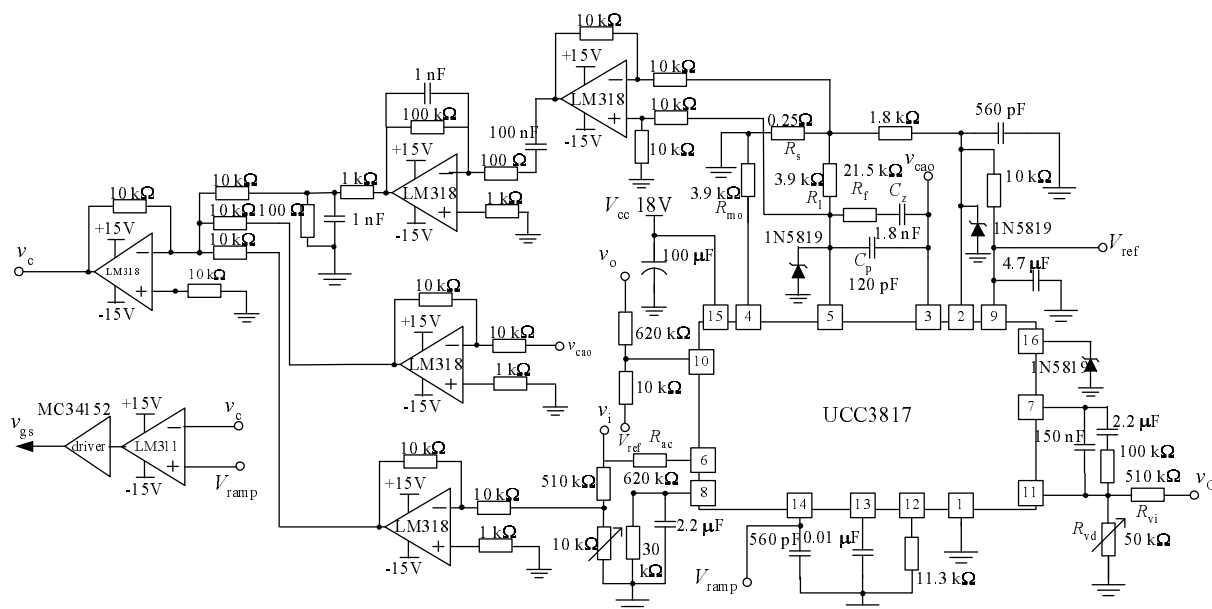


Fig. 5. Schematic of the PFC control circuitry.

VI. EXPERIMENTAL VERIFICATIONS

Two boost PFC converters are constructed to verify the proposed current control rule. One uses the general control rule, which is implemented as feedforward control using a standard LEM controller UCC3817. Another adopts the conventional ACM control using the same controller IC. The complete schematics of the feedforward control are shown in Figs. 5 and 6. The key circuit parameters are shown in Table I.

Comparing Figs. 7 (a) with (b), under line frequency f of 800 Hz, severe zero-crossing distortion is observed under conventional ACM control. Under the general control rule,

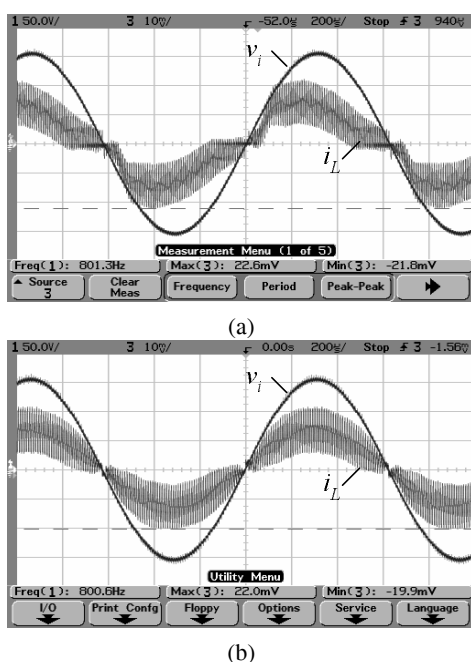


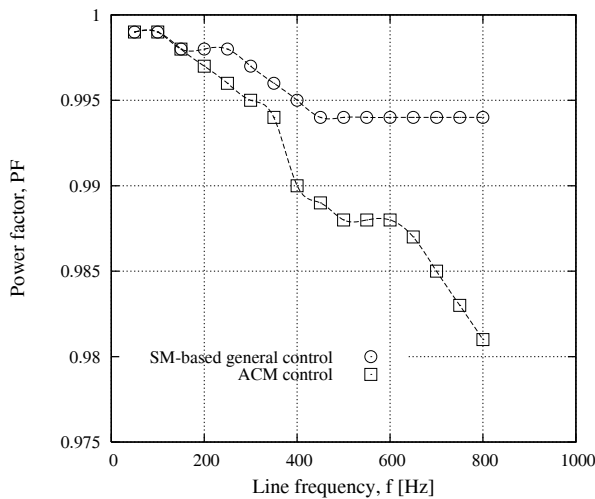
Fig. 7. Inductor current waveforms (500mA/div) resulting from (a) the conventional ACM control and (b) the proposed general control rule. $f = 800$ Hz.

TABLE I
CIRCUIT PARAMETERS USED IN THE EXPERIMENTS

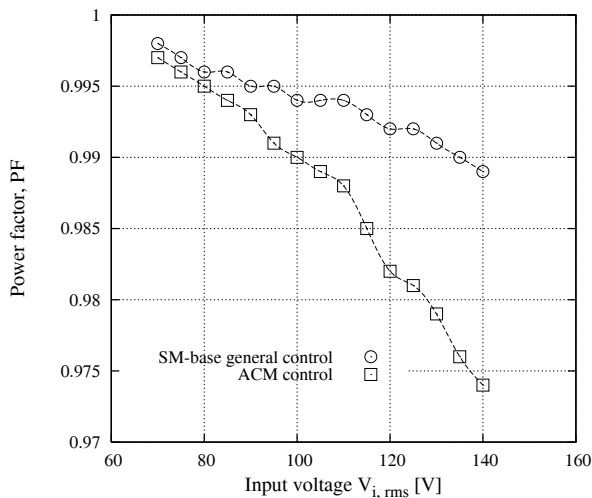
Parameters of PFC stage	Values
Rectified line voltage $V_{i,rms}$	110 V
Nominal line frequency f	500 Hz
Reference output voltage V_{ref}	270 V
Switching frequency f_{sw}	100 kHz
Inductance L	1 mH
Output capacitance C	220 μ F
Nominal resistive load R	1.2 k Ω

low harmonic distortion is observed in the input current. Fig. 8 (a) shows the measured power factor PF of the two converters as f varies from 50 Hz to 800 Hz. Under ACM control, PF drops to around 0.98 at $f = 800$ Hz, while PF under the proposed control is maintained above 0.994. Likewise, as the input voltage $V_{i,rms}$ is increased from 70 Vrms to 140 Vrms, under ACM control, PF drops by 0.03 to around 0.97, while PF of the converter using the proposed control only reduces for less than 0.01, as shown in Fig. 8 (b). This verifies the robustness of the general control against the variation of line frequency and line voltage.

Under the general current control, frequency responses of the current loop are measured and plotted along with the theoretical Bode plots in Fig. 9 (a). Here we intend to demonstrate an unstable current loop and the SM coefficients are chosen such that the phase margin is less than 10° . The measured frequency responses generally agree with the theoretical Bode plots and an oscillation at a frequency coherent to the crossover frequency is observed in the inductor current waveform shown in Fig. 9 (b). The small discrepancies can be attributed to the tolerance of the compensation components and the presence of parasitic components in the power converter, which have not been taken into account in our derivation.



(a)

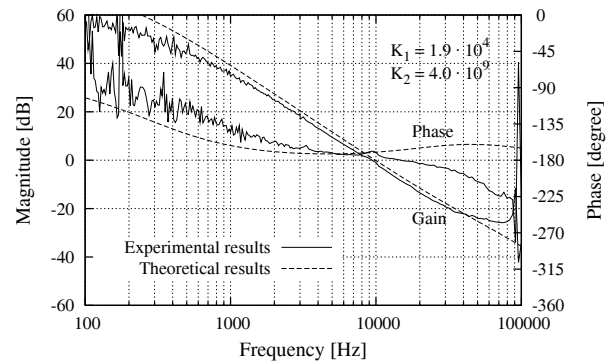


(b)

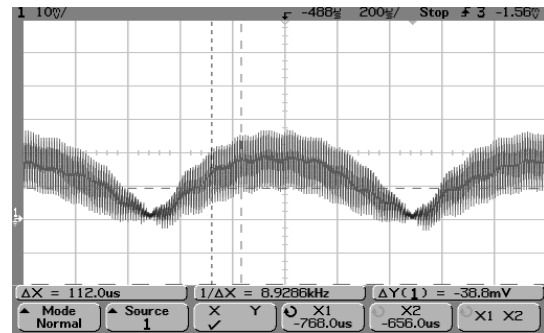
Fig. 8. PF measured over the variations of (a) line frequency and (b) input voltage.

VII. CONCLUSION

In this paper, we have presented the derivation, design and experimental evaluation of a general current control rule for the boost PFC converter. The resulting control rule achieves low input current distortion against the variation of line condition. It takes a common form of PWM control and can be either implemented as an individual controller, or feedforward control applied to a standard PFC controller. SM operation can be ensured by the compliance of the existence condition. The current loop gain is deduced from the sliding surface equation. Stability and performance of the system can be assessed by Bode plots, and based on that the SM



(a)



(b)

Fig. 9. (a) Bode plots of the current loop with an unstable set of SM coefficients; (b) the corresponding inductor current waveform (500 mA/div). $K_1 = 1.9 \cdot 10^4$, $K_2 = 4 \cdot 10^9$.

coefficients can be designed in conjunction with the existence condition. Experimental measurements generally agree with the analytical results. The alleviation of the zero-crossing distortion and the robustness of the proposed control have been verified.

REFERENCES

- [1] J. Sun, "On the zero-crossing distortion in single-phase PFC converter," *IEEE Trans. Power. Electron.*, vol. 19, no. 3, pp. 685–692, May 2004.
- [2] S. C. Tan, Y. M. Lai, C. K. Tse, and K. H. Cheung, "A fixed-frequency pulsewidth modulation based quasi-sliding-mode controller for buck converters," *IEEE Trans. Power. Electron.*, vol. 20, no. 6, pp. 1379–1392, Nov 2005.
- [3] S. C. Tan, Y. M. Lai and C. K. Tse, "Indirect sliding mode control of power converters via double integral sliding surface," *IEEE Trans. Power. Electron.*, vol. 23, no. 2, pp.600 611, Mar. 2008.
- [4] S. Wall and R. Jackson, "Fast controller design for single-phase power-factor-correction systems," *IEEE Trans. Ind. Electron.*, vol. 44, no. 5, pp. 654–660, 1997.
- [5] M. Chen and J. Sun, "Feedforward current control of boost single-phase PFC converters," *IEEE Trans. Power. Electron.*, vol. 21, no. 2, pp. 338–345, Mar 2006.
- [6] L. H. Dixon, "High power factor switching pre-regulator design optimization," *Unitrode Power Supply Design Seminar Manual SEM700*, 1990.